Experimental Mechanics (2006) 46: 179–196
DOI 10.1007/s11340-006-6416-6

An Experimental Study of Mixed Mode Crack Initiation and Growth in Functionally Graded Materials

J. Abanto-Bueno · J. Lambros

Received: 7 July 2005 / Accepted: 15 November 2005

Abstract Quasi-static mixed mode crack initiation and growth in functionally graded materials (FGMs) was studied through fracture experiments on polymer-based FGMs manufactured by selective ultraviolet irradiation of poly(ethylene carbon monoxide)—a photo-sensitive copolymer that becomes more brittle and stiffer under ultraviolet irradiation. The objective of the study was to determine whether crack kinking criteria for homogeneous materials, e.g., maximum hoop stress criterion, also hold for FGMs. Single edge notched tension specimens with different spatial variations of Young's modulus, failure stress and failure strain, were tested. Near tip mode mixity was introduced either by inclining the crack to the remote loading direction, as in the case of homogeneous materials, or to the direction of material gradient, or both. A full-field digital image correlation technique was used to measure in real-time the displacement field around the crack tip while it propagated through the graded material, and to extract the fracture parameters of stress intensity factor K_I and K_{II}, and the T-stress. It was found that the nonsingular T-stress term in the asymptotic expansion for stresses plays a very important role in accurately measuring fracture parameters. It was also found that the maximum tangential stress criterion can be applied to the case of FGMs to predict crack kinking provided that the effect of the T-stress is accounted for and the process zone size is small compared to the intrinsic material gradient length scale. However, for accurate crack path prediction at a length scale comparable to the material gradient, detailed material property information is required. In general, the crack will propagate towards a region that exhibits less fracture toughness, but, unlike the case of homogeneous materials, along a path where K_{II} is not necessarily equal to zero.

Keywords Functionally graded materials · Mixed mode fracture · Digital image correlation · T-stress · Poly(ethylene carbon monoxide)

J. Lambros (✉, SEM member)
Department of Aerospace Engineering,
University of Illinois at Urbana–Champaign, Urbana,
IL 61801, USA
e-mail: lambros@uiuc.edu

J. Abanto-Bueno (SEM member)
Present address: Department of Mechanical Engineering,
Bradley University, Peoria, IL 61625, USA

Introduction

Many quasi-static crack initiation events arise from mixed mode loading occurring in the vicinity of a crack tip. In the case of functionally graded materials (FGMs) such mixed mode conditions can be influenced not only by the orientation of the applied load to the crack (as in homogeneous materials), but also by the orientation of the property gradient direction. There have been several attempts to study mixed mode fracture in FGMs and to determine whether fracture criteria developed for homogeneous materials, such as the maximum hoop (or tangential) stress criterion, $(\sigma_{\theta\theta})_{\max}$ [1] or the maximum strain energy release rate criterion, G_{max}, [2], are also valid for FGMs. Gu and Asaro [3] studied crack deflection in FGMs having a crack perpendicular to the material

elastic gradient, which was assumed to have an exponential variation. They assumed local homogeneity, and a maximum energy release rate criterion and found that when the crack is placed on the compliant side, the energy release is enhanced if the crack kinks towards the more compliant region. In a second work, Gu and Asaro [4] suggested that a crack will propagate when the energy release rate G reaches a critical value G^R, the toughness of the FGM. However they pointed out the necessity of experimentation for a complete understanding of the mixed mode fracture behavior of FGMs.

Two other numerical investigations are relevant to the present work, Becker et al. [5] and Kim and Paulino [6], both of which include the effect of the T-stress (the nonsingular term acting in a direction parallel to the crack plane in the asymptotic expansion for stresses) in their finite element simulations. For homogeneous materials, the T-stress plays an important role in their fracture in absence of localized yielding, or when the size of the plastic zone is small relative to the process zone [7]. For instance Smith et al. [8] showed that positive T-stress reduces the apparent fracture toughness in mixed mode loading and negative T-stress increases it. The role of the T-stress in the fracture behavior of FGMs is less understood. Becker et al. [5], using the maximum energy release rate criterion, found that for FGMs the magnitude of the T-stress is, on average, greater than the one corresponding to homogeneous materials having the same geometry. It was also found that, in contrast to homogeneous materials, for kink angles that maximize the energy release rate the mode II stress intensity factor, K_{II}, is not necessarily zero. Kim and Paulino [6], using a generalized maximum hoop stress criterion that also includes the T-stress, found that positive T-stress values increase the crack initiation angle, and vice-versa, when compared to the homogeneous case. In addition, a significant influence of the FGMs intrinsic degree of nonhomogeneity on the magnitude and sign of the T-stress was observed.

Experimental study of the mixed mode fracture of FGMs lags behind in comparison with both numerical and theoretical efforts. Rousseau and Tippur [9] investigated the fracture behavior of FGMs with cracks perpendicular to the elastic gradient and found that the crack kinked towards the more complaint region, and both the maximum hoop stress and the vanishing K_{II} criteria [10] can also be applied to predict the kinking angle in FGMs. However, the T-stress was not included in their analysis and no connection to local failure properties was made. More recently, Abanto-Bueno and Lambros [11] experimentally measured crack growth resistance curves for model polymer-based FGMs under pure mode I loading and showed that their fracture response is directly influenced by the combined effect of the local failure stress and failure strain.

In the present work the mixed mode fracture response of polymer-based FGMs, and the suitability of using a maximum hoop stress or energy release rate criterion for the case of FGMs are investigated. The mechanical and fracture characterization of FGMs is accomplished using a comprehensive approach which measures local values of Young's modulus E, failure stress σ_f and failure strain ε_f; while also obtaining the mode I and II stress intensity factors and T-stress for each FGM. The effect of both external loading orientation and property gradient orientation on the mixed mode response of the FGMs is also analyzed. Section 2 provides a brief theoretical description of the maximum hoop stress criterion for crack kinking. Details of the material, experimental procedure and analysis methodology are given in Section 3. Results and discussion of mixed mode crack initiation and growth both in the homogeneous and graded materials are presented in Section 4 and conclusions are drawn in Section 5.

Generalized Maximum Hoop Stress Criterion

The maximum hoop stress criterion introduced by Erdogan and Sih [1] can be generalized to include the effect of T-stress [12]. This criterion, which only involves the stress field surrounding the tip in its prediction of crack kinking, states that the crack will kink along the direction in which the hoop stress is maximum. Inclusion of the T-stress in the maximum hoop stress criterion application results in a non-unique kink angle, α, prediction that depends not only on the loading, manifested through the stress intensity factors K_I and K_{II} and the T-stress, but also a length parameter r_c through

$$K_I \sin\alpha + K_{II}(3\cos\alpha - 1) - \frac{16}{3} T\sqrt{2\pi r_c} \times \sin\frac{\alpha}{2}\cos\alpha = 0. \quad (1)$$

If $T = 0$ then equation (1) reduces to the result of Erdogan and Sih [1],

$$K_I \sin\alpha + K_{II}(3\cos\alpha - 1) = 0, \quad (2)$$

which furnishes a unique kink angle based only on the ratio K_{II}/K_I. The kink angle α in equations (1) and (2)

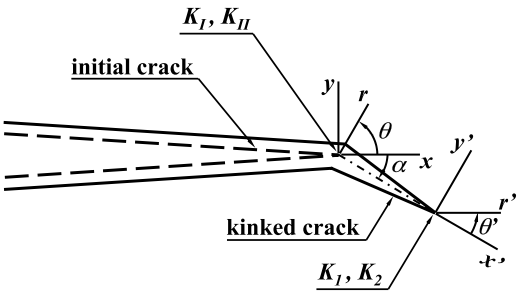

Fig. 1. Coordinate axes at an initial crack tip and the geometry of a kinked crack

is measured with respect to the crack tip as shown in Fig. 1. (K_1 and K_2 are respectively the mode I and II stress intensity factors in the "kinked" prime reference frame.) The parameter r_c is likely related to some microstructural length scale of the material. For the case of a homogeneous material it could be determined experimentally if crack kinking data are available over a large range of mode mixity $\psi = \tan^{-1}(K_{II}/K_I)$. For the FGM case, its computation is not as straightforward since r_c may be a function of position.

Experimental Procedure and Methodology

The material used in this investigation was a 1%wt. CO poly(ethylene carbon monoxide) copolymer, also known as ECO, in form of thin sheets (406 μm thick). ECO is a very ductile (~ 900% failure strain) semicrystalline copolymer that undergoes accelerated mechanical degradation when exposed to ultraviolet (UV) light [13, 14], which makes it well suited to generate quasi-brittle large scale complex heterogeneous materials [15, 16].

Homogeneous Materials

A prerequisite to studying the graded ECO was to establish whether homogeneous ECO subscribed to a maximum hoop stress criterion. ECO sheets were homogeneously irradiated for 50 h and their mechanical properties and fracture parameters were measured from uniaxial tensile tests and single edge notch tension (SENT) fracture experiments performed on a tabletop universal testing Machine (Model Alliance RT/30, MTS Systems Corporation, Eden Prairie, MN). Both the tensile and fracture experiments were conducted under displacement control and a loading rate of 0.5 mm/min. Mixed mode loading was generated by placing the crack at an angle ϕ with respect to the applied loading direction as illustrated in Fig. 2. Table 1 gives the dimensions and crack inclination for

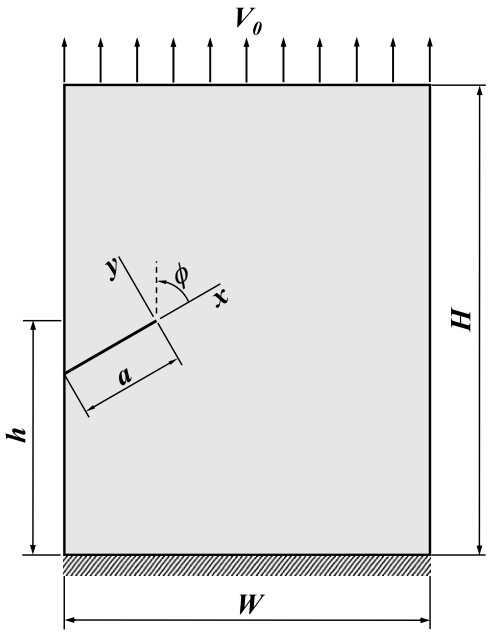

Fig. 2. Mixed mode fracture specimen configuration. V_0, a and ϕ are the applied displacement, initial crack length and crack orientation to the applied displacement

the two cases considered. Before testing, and for subsequent use with the digital image correlation (DIC) technique, a random speckle pattern was sprayed onto one of the surfaces of the SENT specimens using black paint. A 1280 × 960 pixels CCD camera (Model XCD-SX900, Unibrain Inc., San Ramon, CA) was used to image the region around the crack tip for crack extensions up to 20 mm.

A sequence of three representative images from the fracture experiments carried out on specimens HOM I ($\phi = \pi/3$) and HOM II ($\phi = \pi/6$) are shown in Fig. 3(a) and (b) respectively. In both cases, the image at the top of each sequence corresponds to the instant just before crack initiation, while the next two images show the crack path followed (the crack tip is identified by an arrow). In both cases the crack kinked off the initial crack plane but at two different angles α.

Functionally Graded Materials

The technique of Lambros et al. [14] and Abanto-Bueno and Lambros [17] to manufacture model

Table 1 Dimensions and loading conditions of the SENT specimens used in the mixed mode fracture tests of homogeneously irradiated ECO

	H (mm)	W (mm)	h (mm)	a (mm)	ϕ (rad)
HOM I	90	70	45	33	π/3
HOM II	90	70	45	40	π/6

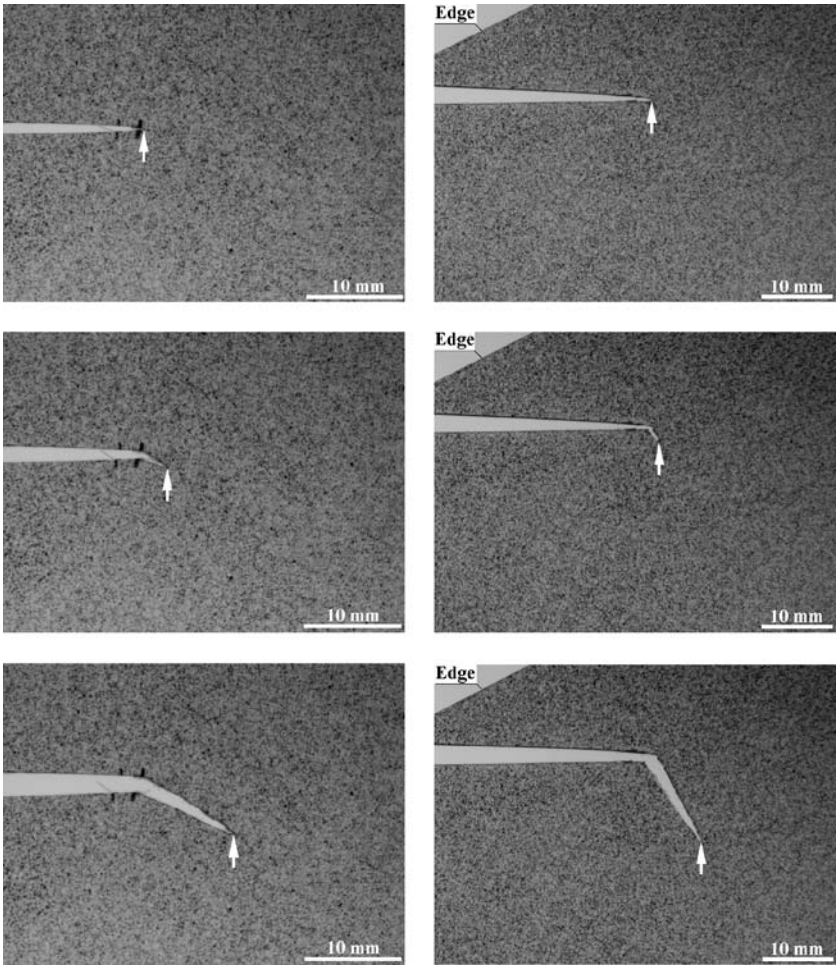

Fig. 3. Representative digital images recorded during the fracture tests performed on (**a**) HOM I ($\phi = \pi/3$), and (**b**) HOM II ($\phi = \pi/6$). Crack tip location is identified by an arrow

ECO-based functionally graded materials was also used here. This technique exploits the ductile-to-brittle transition of ECO under UV light exposure to generate functionally graded materials by gradually increasing the exposure time on ECO samples as a function of their width. The resulting material possesses a graded region of continuous property transition from a ductile mechanical response (short irradiation times) to a more brittle, stiffer and stronger response (long irradiation times).

Mixed mode loading in FGMs can be attained either by asymmetric external loading, as in the homogeneous material, or by placing the crack line at an angle to the direction of mechanical property variation, or by a combination of both. The effect of each of these cases was investigated using four specimens labeled here FGM I, II, III, and IV. Every graded ECO sheet was cut in two identical halves (samples) along the material property gradient direction. One half was used to measure the spatial variation of Young's modulus E, failure stress σ_f and failure strain ε_f for each FGM sheet by performing uniaxial tensile tests on 8–10 mm wide strips cut perpendicularly to the material property gradient direction and along the entire width of the FGM sample. The measured variation of E, ε_f and σ_f along the widths of FGMs I to IV are shown in Fig. 4(a.1) to (d.1), respectively. Fitted trend lines to the measured data have also been included in these figures. The other half of the FGM sheet was used to generate SENT fracture specimens. The final dimensions of the fracture specimens were constrained by the (desired) mixed mode loading conditions, crack tip position, and the original dimensions of the ECO sheet. Mixed mode loading conditions for each fracture specimen were defined by ϕ, the angle between the initial crack line and the direction of applied load, and γ, the angle between the crack and property gradient direction. Figures 4(a.2) to (d.2) show the final geometry of the SENT fracture specimens for FGMs I to IV and their actual dimensions are given in Table 2. In order to identify the properties at the initial crack tip,

the distance to the stiffer edge of the initial FGM sample [left edge in Fig. 4(a.1)–(d.1)], measured parallel to the property gradient direction, has been also included in Table 2.

FGMs I and IV have symmetric loading with respect to the crack tip, but mixed mode conditions are still expected to occur at the initial crack tip because of a 90° inclination of the material gradient with the crack line. This configuration will therefore allow us to study the importance of mixed mode effects as introduced by the material gradient. Note that although FGMs I and IV generate apparently the same type of mixed mode loading conditions, the crack tip has been positioned in regions where their σ_f and ε_f have different spatial behavior. This was done in order to investigate the influence of fracture parameters σ_f and ε_f on the crack kinking behavior. For a material of homogeneous toughness, these parameters will not affect crack kinking and a criterion based solely on the applied mechanical fields is sufficient. For a crack lying on a discrete interface between two dissimilar solids, it is clear that crack kinking will be influenced not only by the stress field around the crack tip, but also by the relative toughness of each constituent and of the interface. For example, even if the maximum hoop stress criterion predicts kinking, say, above the interface, if that constituent is extremely tough this will not occur and the crack would then be forced to grow along a direction where $\sigma_{\theta\theta}$ (or G) is *not* maximum. In such a case the criterion employed would be a comparison of available stress (or energy) quantities with the local toughness values. In the case of an FGM, where there

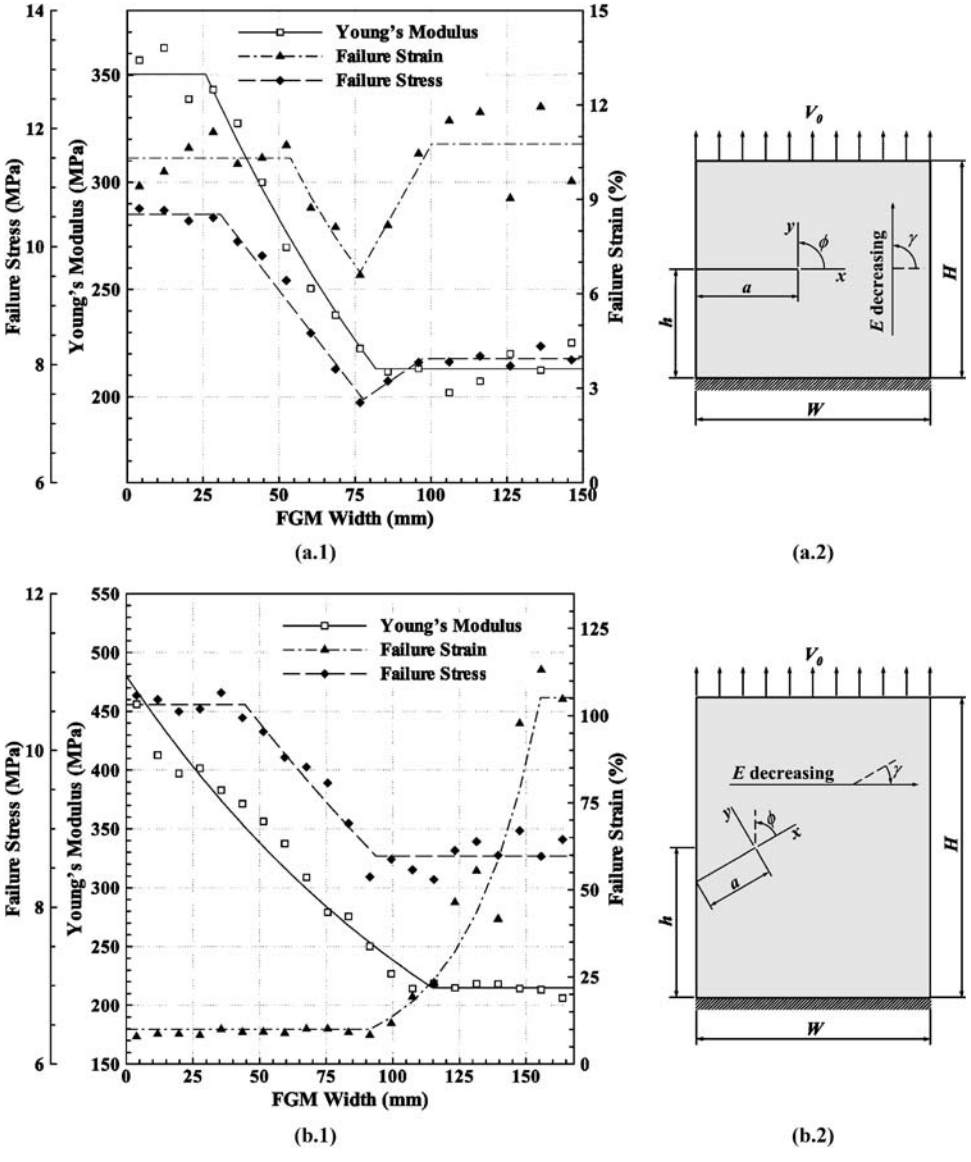

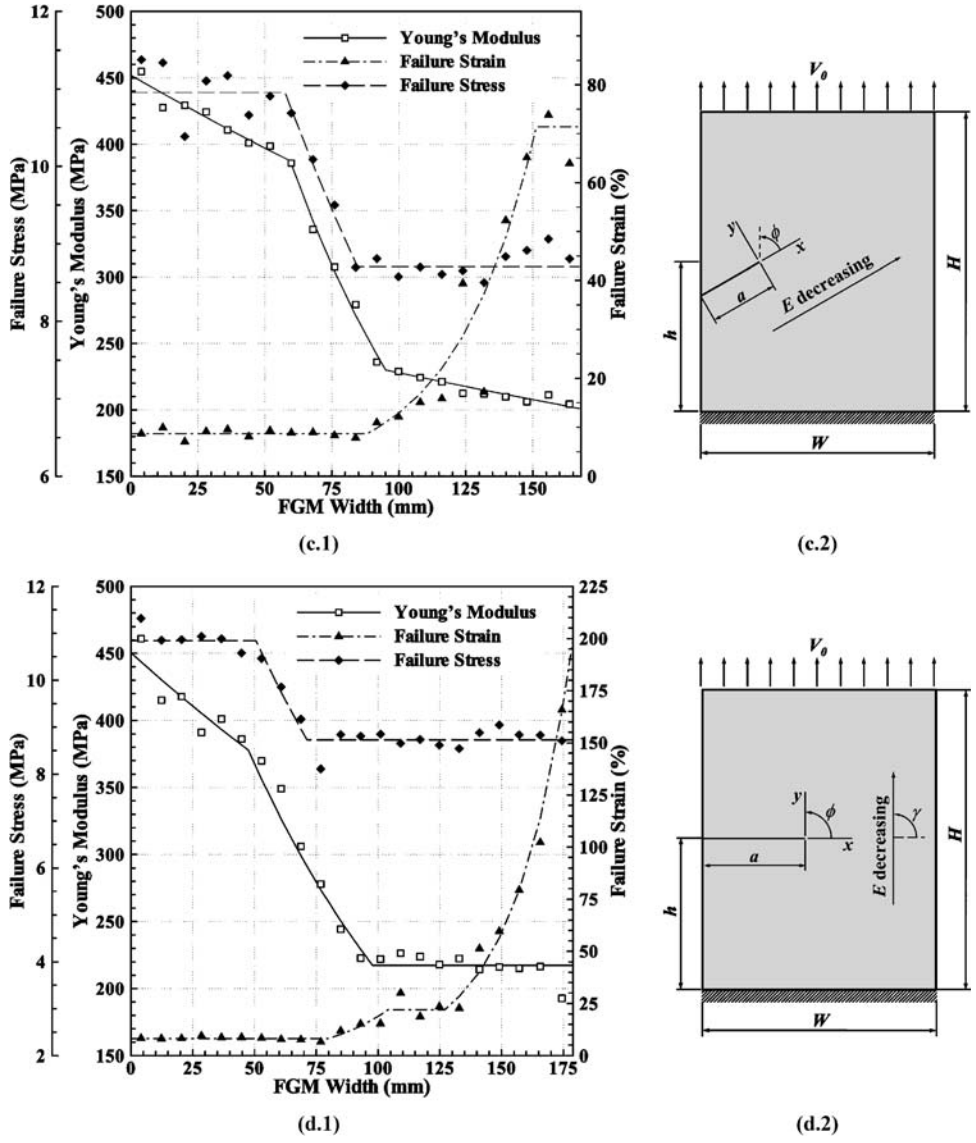

Fig. 4. Measured values of E, σ_f and ε_f as a function of the width of (**a.1**) FGM I, (**b.1**) FGM II, (**c.1**) FGM III, and (**d.1**) FGM IV. Fitted lines for each FGM property have also been included. (**a.2**)–(**d.2**) SENT fracture specimens geometry and loading conditions for FGMs I–IV, respectively. The crack tip was located at a distance of (a) 52 mm (b) 43 mm, (c) 57 mm and (d) 95 mm from the stiffer end respectively

is a continuous variation of properties around the crack tip, one would expect this effect to be pronounced if the material gradient is very steep—probably on the order of the fracture process zone size. This idea guided the use of FGMs I and IV since FGM IV is such that the material property gradient in the vicinity of the initial crack tip is much more severe than in FGM I.

Table 2 Fracture specimen dimensions and crack orientation used in the mixed mode fracture experiments of FGMs

	FGM Specimen dimensions*					Crack* orientation	
	H (mm)	W (mm)	h (mm)	a (mm)	Tip position from stiffer edge (mm)	ϕ (rad)	γ (rad)
FMG I	75	70	32.5	30	52	$\pi/2$	$\pi/2$
FGM II	90	70	45	26	43	$\pi/3$	$-\pi/6$
FGM III	90	70	45	25	57	$\pi/3$	0
FGM IV	100	75	50	33	95	$\pi/2$	$\pi/2$

*See Fig. 4(a)–(d)

FGM II is such that the crack is inclined both with respect to the applied loading and the material property gradient producing mode mixity at the tip from both sources. Finally, in FGM III the crack is parallel to the material gradient, but still at an angle to the applied loading, producing mixed mode loading from far-field loading only, at least until the crack kinks.

Four representative images from the fracture experiments performed on FGMs I, II and III are shown in Fig. 5(a)–(c) respectively. The image at the top of each sequence corresponds to the instant *just before* crack initiation, the two middle images were taken during crack growth and the fourth image was taken immediately after the fracture experiments to show the entire fracture path and the corresponding kink angle α. For reference the external loading angle ϕ has also been included in this figure. From Fig. 5(a) we can see that even though symmetric external load was applied in FGM I, the crack clearly kinked showing the direct effect of the FGM property gradient orientation on the chosen crack propagation path. It is important to mention, however, that in this case the crack extended straight ahead for about 2 mm before kinking. In addition, after the 2 mm growth, the kink angle is surprisingly small despite the large angle between gradient direction and initial crack line. The effect of the property gradient orientation is also noticeable, in a less pronounced fashion, in the other two FGMs in which the paths followed by the cracks were different, even though the experiments were performed under identical external applied load conditions ($\phi = \pi/3$). Also it is worth pointing out that the crack paths followed in FGMs I and III [Fig. 5(a) and (c)] were curved, while in FGM II the crack essentially remained straight after kinking.

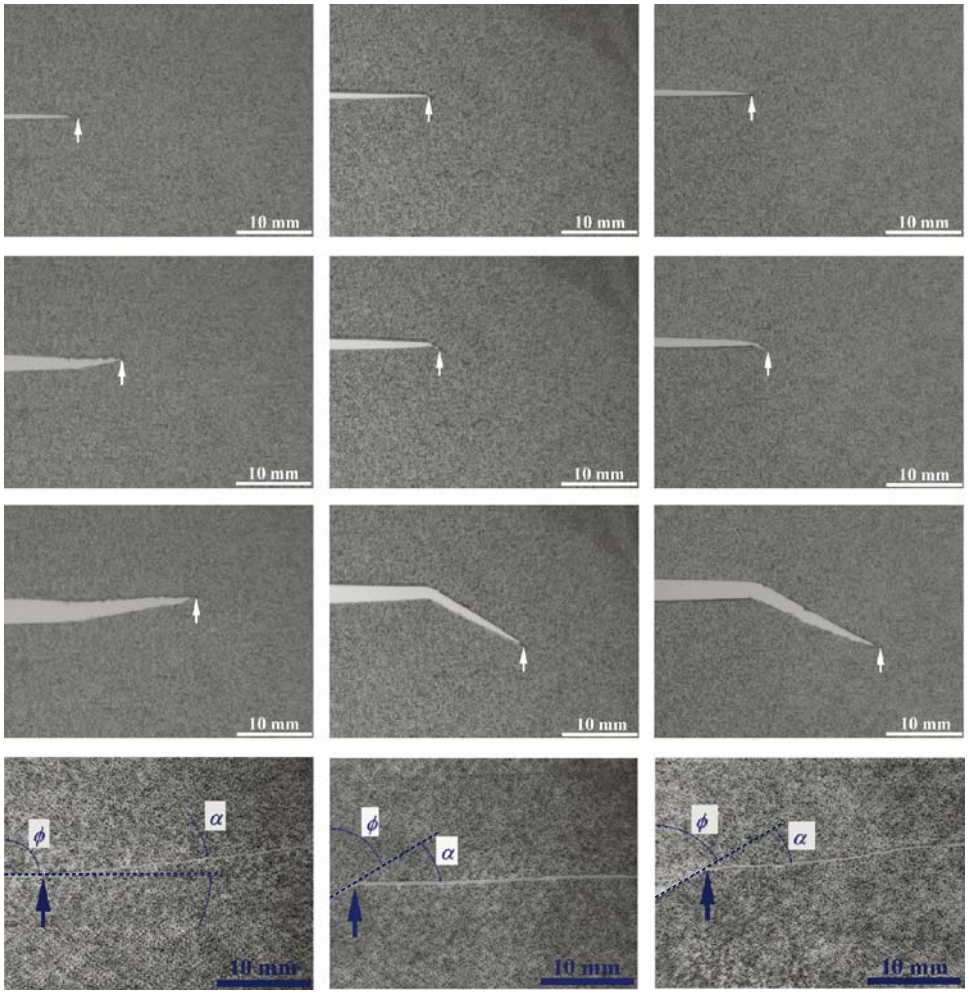

Fig. 5. Representative digital images recorded during the fracture experiments performed on (**a**) FGM I, (**b**) FGM II, and (**c**) FGM III. Crack tip location is identified by an arrow

Digital Image Correlation

The digital image correlation (DIC) method is a full-field optical technique used to accurately measure deformation (displacement and strain) fields by comparing the local features of digital images taken before and after deformation of a random speckled surface of the solid body under investigation. Details of the method can be found in the literature (e.g., [18, 19]) and will not be discussed here. In this investigation, a hybrid DIC scheme, which combines the two most accepted DIC minimization methods available in the literature, the Coarse-fine [18] and Newton–Raphson [19] methods, was implemented to measure in-plane displacements and strains in three consecutives steps. The first step is a variant of the Coarse-fine method and gives an approximate measurement of the displacement field by neglecting displacement gradients. In the second step, an approximate strain field is determined by numerically differentiating the displacement field obtained in step one. In the third step, commonly known as the Newton–Raphson approach, the actual displacement and strain fields are measured using as initial conditions the approximate displacement and strain fields obtained from steps one and two, respectively.

Extraction of Fracture Parameters

Following McNeil et al. [20], the DIC measured displacement field was used to extract fracture parameters by performing a least square minimization of the asymptotic expressions of the displacement field around a crack tip. For linear elastic continuously non-homogeneous materials the asymptotic fields around a crack tip have the same functional form as in the case of homogeneous materials, but with material properties evaluated at the crack tip position [21]:

$$u_x = \underbrace{\frac{K_I}{2\mu_{tip}}\left(\frac{r}{2\pi}\right)^{\frac{1}{2}}\cos\frac{\theta}{2}\left(\frac{3-\nu_{tip}}{1+\nu_{tip}}-\cos\theta\right)+\frac{2C_{12}}{\mu_{tip}(1+\nu_{tip})}r\cos\theta}_{\text{Mode I loading}} + \underbrace{\frac{K_{II}}{4\mu_{tip}}\left(\frac{r}{2\pi}\right)^{\frac{1}{2}}\left[\frac{9+\nu_{tip}}{1+\nu_{tip}}\sin\frac{\theta}{2}+\sin\frac{3\theta}{2}\right]+\frac{2C_{22}}{\mu_{tip}(1+\nu_{tip})}r\sin\theta}_{\text{Mode II loading}}$$
$$- \underbrace{A_1 r\sin\theta + u_{0x}}_{\text{Rigid body motion}} + H.O.T., \tag{3}$$

$$u_y = \underbrace{\frac{K_I}{2\mu_{tip}}\left(\frac{r}{2\pi}\right)^{\frac{1}{2}}\sin\frac{\theta}{2}\left(\frac{3-\nu_{tip}}{1+\nu_{tip}}-\cos\theta\right)-\frac{2C_{12}\nu_{tip}}{\mu_{tip}(1+\nu_{tip})}r\sin\theta}_{\text{Mode I loading}} + \underbrace{\frac{K_{II}}{4\mu_{tip}}\left(\frac{r}{2\pi}\right)^{\frac{1}{2}}\left[\frac{5\nu_{tip}-3}{1+\nu_{tip}}\cos\frac{\theta}{2}-\cos\frac{\theta}{2}\right]-\frac{2C_{22}}{\mu_{tip}(1+\nu_{tip})}r\cos\theta}_{\text{Mode II loading}}$$
$$+ \underbrace{A_1 r\cos\theta + u_{0y}}_{\text{Rigid body motion}} + H.O.T., \tag{4}$$

where u_x and u_y are displacement components parallel and normal to the crack line, respectively, K_I and K_{II} are the mode I and mode II the stress intensity factors, respectively, and μ_{tip} and ν_{tip} are the local shear modulus and Poisson's ratio at the crack tip, respectively. C_{12} is a constant proportional to the nonsingular T-stress parallel to the crack plane ($T = 4C_{12}$), C_{22} is an integration constant which does not affect either the strain or the stress field, A_1 defines rigid body rotation (same effect as C_{22}), and u_{0x} and u_{0y} represent rigid body translation along the x- and y-directions, respectively.

The effect of ν_{tip} has been shown theoretically to be almost negligible in FGMs under remote loading [22]. Here the value of $\nu = 0.45$, measured in Abanto-Bueno and Lambros [10, 23], is used throughout. Once K_I and K_{II} have been measured the kink angle α can be predicted for the case of homogeneous materials, and possibly for the case of FGMs, using the maximum hoop stress criterion outlined in Section 2. The polar coordinates (r,θ) used in equations (3) and (4) and the kink angle α are defined in Fig. 1.

Results and Discussion

Homogeneous Materials

Prior to studying the FGM we wished to establish whether the (generalized) maximum hoop stress criterion was suitable to predict crack kinking in homogeneously irradiated ECO. Both crack initiation and growth under mixed mode loading was studied for 50 h homogeneously UV irradiated ECO for the HOM I ($\phi = \pi/3$) and HOM II ($\phi = \pi/6$) samples.

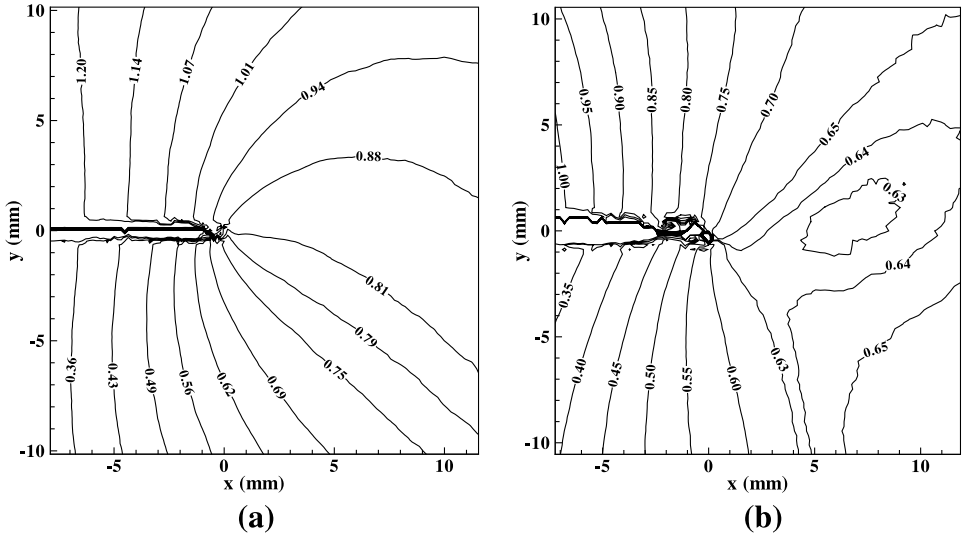

Fig. 6. Normal (to the crack line) displacement field just before crack initiation measured using the DIC technique from the images taken during the mixed mode fracture tests of (**a**) HOM I and (**b**) HOM II. Displacement contours in mm

Crack initiation

The DIC measured u_y displacement component *just before* crack initiation for specimens HOM I and HOM II is shown in Fig. 6(a) and (b) respectively. Although the raw DIC data also include the effect of rigid body motion, the field is clearly asymmetric indicating mixed mode loading at the tip. The significant difference between HOM I and II results can be attributed to the interaction between the crack tip and the edge of the specimen in HOM II resulting from a steeper crack.

To determine the effect of T-stress on K_I and K_{II} the least square minimization of DIC data was carried out by assuming both $T = 0$ and $T \neq 0$ in equation (4). The results of both minimizations are given in Table 3. For HOM I the measured value of the (compressive) T-stress is relatively small and there little change in K_I and K_{II} upon inclusion of the T-stress. For HOM II, in which the crack is more inclined towards the free edge, there is a significant change, especially in K_I, when T-stress is included. In addition, the T-stress itself is much larger and has changed sign, a fact which has also been seen in the numerical simulations of Becker et al. [5] and Kim and Paulino [6] who determined that $\phi = \pi/4$ is the loading angle at which the T-stress sign changes.

The quality of the least square minimization process was evaluated by comparing the measured and theoretical crack tip displacement fields. The former is the result of subtracting the rigid body motion field (after substituting the fitted coefficients) from the DIC measured displacement, and the latter is the asymptotic displacement field expression using the least square calculated coefficients. Contour plots of the u_y measured displacement field (dash-dotted line) and the corresponding theoretical one (continuous line) are shown in Fig. 7(a) ($T = 0$) and (b) ($T \neq 0$), for HOM II. This figure shows the need to account for T-stress in HOM II in order to accurately described the measured displacement field. For HOM I there is only a small improvement in the quality of the fit when the T-stress is included.

Using the measured values of stress intensity factors at the time of crack initiation without including the T-stress effect, kink angle can be predicted using the maximum hoop stress criterion (equation 2). The results of this prediction for HOM I and II are given in the right hand side of Table 4 (for $T = 0$) along with the actual crack kink angle α measured experimentally. The kink angle predicted using the maximum energy release rate criterion, as taken from Becker et al. [5], and the near-tip mode mixity ψ (=$\tan^{-1}(K_{II}/K_I)$) are also included in the table. The error in the

Table 3 Results of the least square minimization for $T = 0$ and $T \neq 0$ for homogeneous ECO

	$T \neq 0$			$T = 0$	
	K_I (MPam$^{0.5}$)	K_{II} (MPam$^{0.5}$)	T (MPa)	K_I (MPam$^{0.5}$)	K_{II} (MPam$^{0.5}$)
HOM I	0.903	0.245	−0.784	0.965	s0.242
HOM II	0.745	0.526	5.536	0.297	0.561

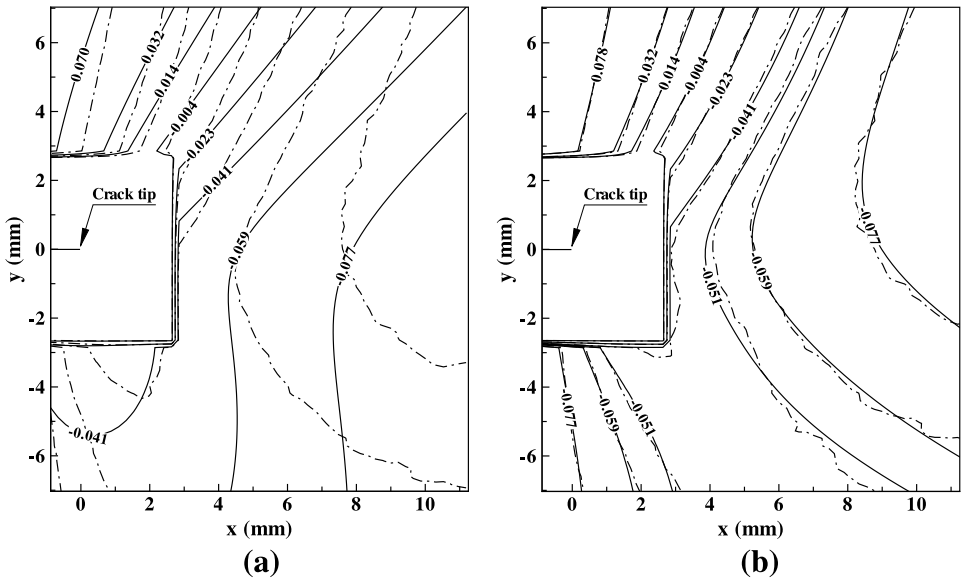

Fig. 7. Contour plots comparing the normal (to the crack line) measured (dash-dotted line) and theoretical (continuous line) crack tip displacement field in HOM II just before crack initiation. The displacement fields were obtained by assuming (**a**) $T = 0$ and (**b**) $T \neq 0$

theoretical prediction of the maximum hoop stress criterion is significant, especially for sample HOM II which has a larger T-stress component. An improvement in this prediction might be to use the *generalized* maximum hoop stress criterion (equations 1), but this requires knowledge of the length scale r_c. Since we essentially have only one data point to extract this length scale from (the HOM II case) it is not possible to use the generalized hoop stress criterion directly in the form of equations (1). (Using the measured values of K_I, K_{II}, T and α in HOM II to computed r_c yields r_c = 50 μm.) Therefore a modification of the generalized maximum hoop stress criterion, in which equation (2) is used to predict the kink angle but with values of stress intensity factor computed *when including the T-stress*, was employed. The results of this prediction are also shown in Table 4 in the column corresponding to $T \neq 0$. The kink angle prediction in both cases, but especially for HOM II, has been improved, confirming the importance of taking into consideration the effect of the T-stress.

Crack growth

For the case of a growing kinked crack, He and Hutchinson [10] found that in homogeneous materials the crack will propagate along the plane that maximizes K_1 and has $K_2 = 0$. In the present experiments K_1 and K_2 were measured for different extensions of the (kinked) crack for both HOM I and II. Figure 8 shows the measured values of K_1 and K_2 as a function of crack extension up to 18 mm for the two homogeneous specimens. In both cases K_2 is almost zero ($< \pm 0.08$ MPam$^{0.5}$) and $K_1 = K_{IC}^{SS}$ (the steady state fracture toughness in mode I of the same material measured in Abanto-Bueno and Lambros [23]), which agrees well, within experimental error, with the results of He and Hutchinson [10].

Table 4 Comparison of actual and predicted kinking angle based on $(\sigma_{\theta\theta})_{\max}$ and $G_{\max}$ criteria

	Actual kinking angle, α (°)	$T \neq 0$				$T = 0$			
		ψ (°)	Predicted α (°)			ψ (°)	Predicted α (°)		
			$(\sigma_{\theta\theta})_{\max}$	$G_{\max}^{**}$	Error* (%)		$(\sigma_{\theta\theta})_{\max}$	$G_{\max}^{**}$	Error* (%)
HOM I	−28 ± 1.5	15.2	−26.9	−27	4.9	14.1	−25.4	−25.5	9.3
HOM II	−52 ± 1.5	35.2	−47.9	−49	7.9	62.1	−60.8	−65	16.9

*Compared to the tangential maximum stress criterions
**Taken from Becker et al. (2001)

Table 5 Measured fracture parameters and corresponding predicted kinking angle based on $(\sigma_{\theta\theta})_{max}$ and G_{max} criteria for FGMs

	Actual kinking angle, α (°)	Minimization measured fracture parameters				Predicted kinking angle, α (°)	
		K_I (MPam$^{0.5}$)	K_{II} (MPam$^{0.5}$)	T (MPa)	ψ (°)	$(\sigma_{\theta\theta})_{max}$	G_{max}*
FGM I	0 (Δa = 0 mm)	0.554	0.039	−4.272	4.0	−7.9	−8
	7 ± 1.5 (Δa = 2 mm)	0.876	0.089	−6.276	5.8	−11.4	−11
FGM II	−28 ± 1.5	0.755	0.179	−0.069	13.3	−24.2	−24
FGM III	−19 ± 1.5	0.969	.224	−0.93	13.0	−23.8	−24

*Taken from Becker et al. [5]

Functionally Graded Materials

Crack initiation

In order to determine whether the crack kinking criteria used in homogeneous materials can be also applied to FGMs, the first image in each sequence of Fig. 5 for FGMs I, II and III was analyzed. The measured values of K_I, K_{II}, T and α and the corresponding predictions from equations (2) and the maximum energy release rate criterion [5] are presented in Table 5. Since in the case of FGM I the crack extended straight ahead for 2 mm before kinking by 7°, the measured values both at the initial tip and just before kinking have been included in the table. From this table we can see that both criteria predict reasonably well the kink angle for FGMs II and III, but not for FGM I where mixed mode conditions were generated solely by the FGM property gradient orientation. It was expected that by using a large property gradient misorientation ($\gamma = \pi/2$), severe mixed mode loading conditions would be created at the crack tip. However, as can be seen in Table 5, the value of K_{II} for FGM I is quite small—almost comparable to the values measurable in a nominally mode I experiment. The sign of K_{II} is responsible for the incorrect prediction of the direction of crack kinking for FGM I. The results for FGM I point to the fact that material inhomogeneity effects are not very significant for crack initiation when the material gradient is much larger than the process zone size occurring at the crack tip. In FGM I the intrinsic gradient length scale is approximately 50 mm while a typical process zone (craze) size for this material is about 1 mm [23]. FGM IV, a sample with the same geometry as FGM I but with a much steeper gradient of failure properties, was manufactured to investigate further the effect of material gradient on crack initiation. The results are described in Section 4.3.

For FGMs II and III the experimental results show that both the generalized maximum hoop stress and the maximum energy release rate criteria as used for homogeneous materials can predict crack kinking

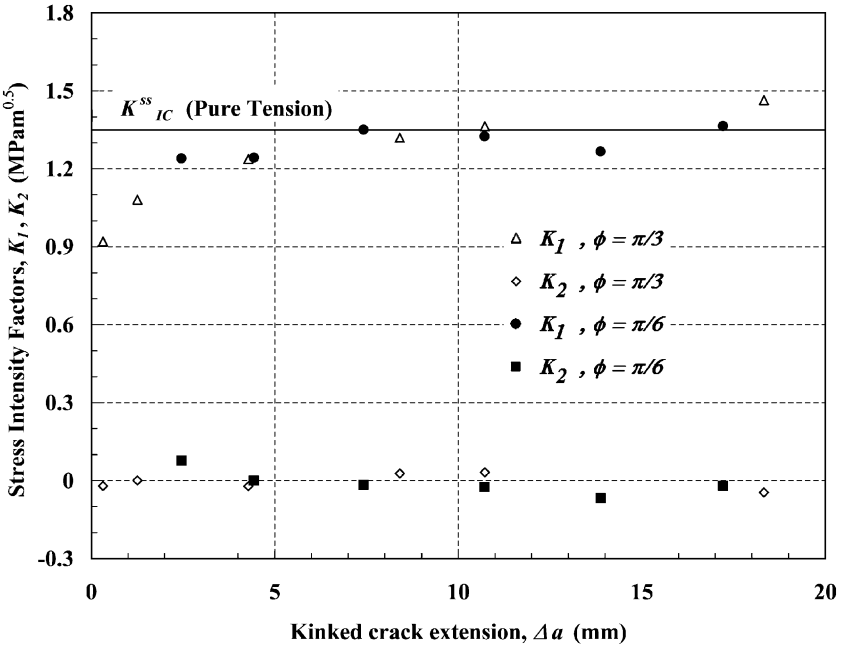

Fig. 8. Measured stress intensity factors K_1 and K_2 versus kinked crack extension for HOM I ($\phi = \pi/3$) and HOM II ($\phi = \pi/6$)

quite well. Unlike the case of interfaces, these criteria involve only the stress field developed around the crack tip. The lack of the need to use local material toughness information for the FGM case can be rationalized since for a material with *continuous* property variation asymptotically to the crack the material will appear homogeneous. In a (mathematical) interface, however, no matter how close we are to the interfacial crack tip, the interface will always be present and the crack tip will always have a choice of three possible growth directions (above, along and below the interface). The present results, therefore, point to the fact that for infinitesimal crack kinking if the fracture process zone responsible for kinking occurs at a length scale that is small compared to the intrinsic material gradient variation, then the homogeneous criteria can be applied—albeit with the inclusion of the *T*-stress effect when necessary.

Crack growth

The effect of the property variation may be more pronounced as the crack propagates through the graded region, when the distance of growth from the initial pre-crack becomes comparable to the intrinsic material gradient length scale. The results for FGM I seem to reinforce this since the crack initially grows straight, but then decidedly turns. The path followed by the propagating crack was digitized and is presented in Fig. 9 for FGMs I, II and III. The *x*-axis coincides with the initial crack line (dash-dotted line) and the origin with the initial crack tip. For FGM I and III the crack continuously followed a curved path, while for FGM II it propagated along a straight line after kinking.

To investigate the influence of local properties of modulus E, failure stress σ_f and failure strain ε_f on crack evolution in the vicinity of the initial crack tip we have plotted contours of $\sigma_{\theta\theta}$ at crack initiation in Fig. 10(a) and (b) for FGM I, and (c) and (d) for FGM II and FGM III. Corresponding isoclines of ε_f (dashdotted lines), and σ_f (longdashed lines), also available from our experiments, have been overplotted on the $\sigma_{\theta\theta}$ contours. For FGM II and III, ε_f is constant everywhere in the region of interest. The values of $\sigma_{\theta\theta}$ plotted in Fig. 10 have been computed by taking both components of the measured DIC full-field displacements, differentiating them to obtain all in-plane strain components, then using the (experimentally known) inhomogeneous material stress–strain relation to evaluate all stress components and, finally, rotating the components to obtain $\sigma_{\theta\theta}$. The stress values differ from those used in prediction of initial crack kinking discussed above since we now have included the effect of varying elastic modulus in the near tip region.

For FGM I, where the material gradient is perpendicular to the initial crack line and symmetric loading is applied, both failure stress and failure strain decrease above the initial crack. The crack does indeed curve upwards [as seen in Fig. 5(a)], i.e., into the area of lower failure properties, opposite from the prediction of the (homogeneous) criteria applied asymptotically at the crack tip (Table 5). It is worth pointing out however, that when the effects of modulus inhomogeneity are included in the computation of $\sigma_{\theta\theta}$ as

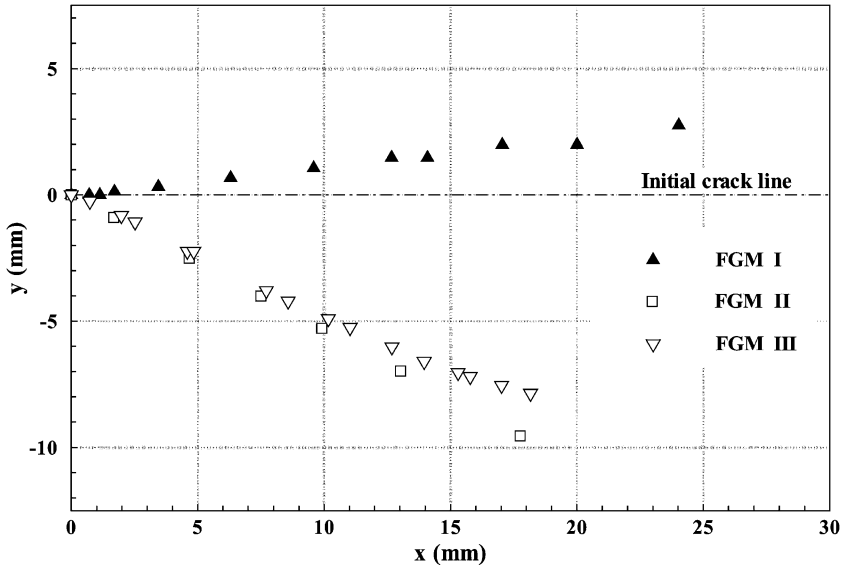

Fig. 9. Path followed by the propagating crack in FGMs I, II and III

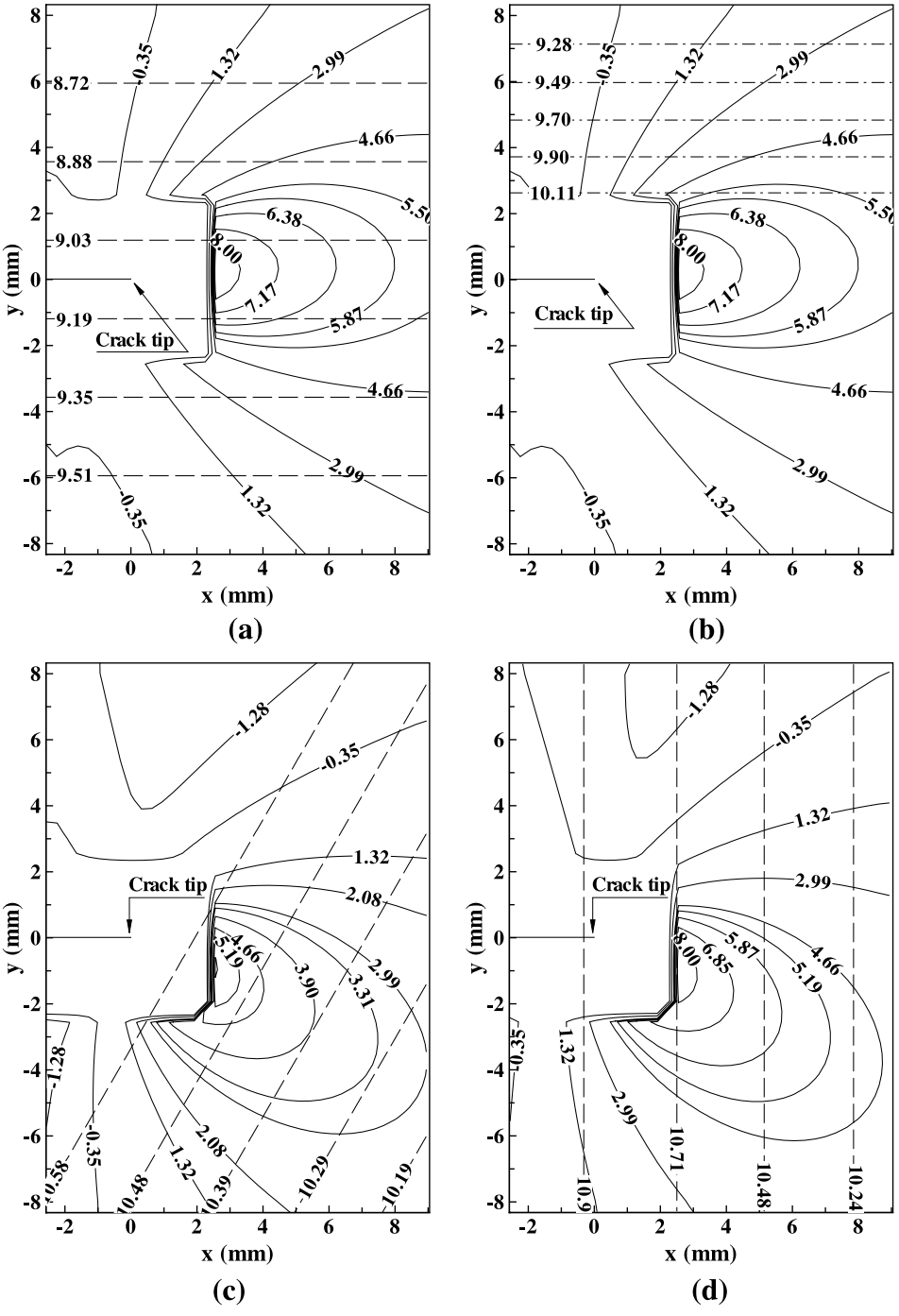

Fig. 10. Contours of (**a**) $\sigma_{\theta\theta}$ and σ_f and (**b**) $\sigma_{\theta\theta}$ and ε_f for FGM I, (**c**) $\sigma_{\theta\theta}$ and σ_f for FGM II, and (**d**) $\sigma_{\theta\theta}$ and σ_f for FGM III. ε_f is in percentage, and $\sigma_{\theta\theta}$ and σ_f in MPa

in Fig. 10(a,b) then the maximum hoop stress is at about 5° for r = 5 mm, which is closer to the actual kink angle of 7° than the prediction of Table 5.

In the case of FGM II, although the initial crack was orientated at an angle with respect to both the applied load and the property gradient, the tip of the crack was located in a region were both ε_f and σ_f are constant [see Fig. 10(c)] and, as seen earlier crack kinking was controlled exclusively by the applied load causing an infinitesimal kink to occur along the maximum tangential stress direction. In this case after the crack kinked it become perpendicular to the applied loading and parallel to the material gradient so that mode I loading conditions occurred thereafter. Therefore the (kinked) crack continued propagating along the same straight path as can be seen in Figs. 9 and 10(c) since it had no incentive to curve. (As will be seen later $K_2 = 0$ during propagation in this case.)

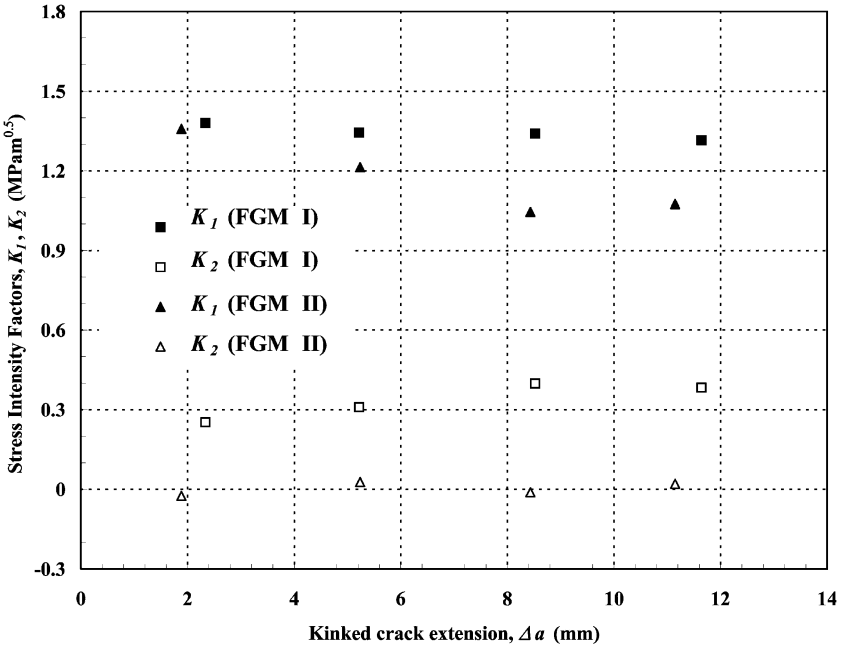

Fig. 11. Measured stress intensity factors K_1 and K_2 versus kinked crack extensions for FGM I and II

The results from FGM III reinforce our previous findings: the crack kinked along the direction of maximum tangential stress and propagated toward the region that possessed less resistance to fracture, but higher elastic modulus. From Fig. 10(d), we can see that because of the orientation of the property gradient direction with the *kinked* crack, a region just in front and above of the crack tip possesses slightly smaller values of ε_f (and thus less fracture resistance) than the region below the crack tip causing the crack to grow towards this region in a continuous, but smooth, fashion as can be seen in the images of Fig. 5(c).

As in the case of homogeneous materials, K_1, K_2 and T were also measured at different extensions of the kinked crack to determine whether the condition of $K_2 = 0$ along the propagating path is also satisfied in FGMs. Results for FGMs I and II are shown in Fig. 11. For FGM II, unlike homogeneous materials, K_1 decreases as the crack grows (since the local material toughness continuously decreases) and, like homogeneous materials, K_2 is almost zero because, as mentioned above, the crack had no incentive to continue curving after kinking since it attained a symmetric configuration. In contrast, for FGM I although K_1 also decreases during growth, $K_2 \neq 0$ and in fact increases as the crack curves from continually changing near tip mixed mode conditions. Similar results of continually changing K_2 were seen in FGM III which also continually curved. Therefore, in stark contrast to homogeneous materials, it is quite possible for stable quasi-static *mixed mode crack growth* in which $K_2 \neq 0$ to occur in FGMs.

FGMs Possessing Steeper Property Gradient

Several FGMs with much steeper property gradient than that of FGM I were manufactured and tested using the configuration shown in Fig. 4(d.2). The aim

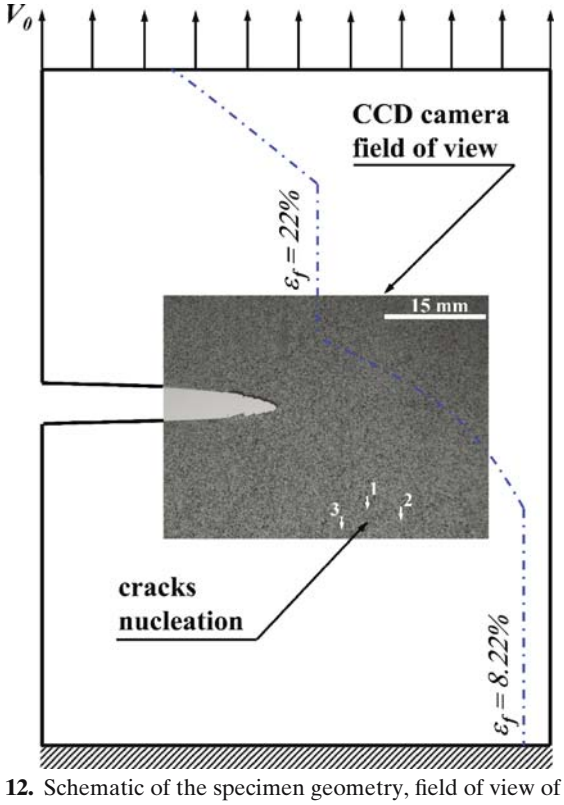

Fig. 12. Schematic of the specimen geometry, field of view of the CCD camera and the location of cracks nucleation during the fracture test performed using FGM IV. The variation of ε_f (dash-dotted line) is also shown schematically

was to generate a situation where the material gradient length scale was comparable to the process zone scale (in the case of 50 h irradiated ECO about 1 mm as seen in Abanto-Bueno and Lambros [23]). However, in most of these cases the crack did not kink at all and the specimens suddenly failed in, or very close to, the grips of the testing machine, where the more brittle (and stiffer) region of the fracture specimen was located. In the fracture experiment performed using FGM IV, however, because of the particular gradient of that specimen, failure occurred far from the grips and in an area still within the field of view of the CCD camera. This allowed us to record, not crack kinking, but the processes of spontaneous nucleation of new cracks, and their growth and coalescence. Figure 12 shows a schematic of the FGM IV specimen, the field of view of the CCD camera, and the location of crack nucleation locations (marked by arrows 1, 2, and 3) as load was increased during the test. In addition the variation of ε_f, along the specimen height, is over plotted schematically [the actual distribution is shown in Fig. 4(d.1)].

Four selected CCD images and the corresponding contour plots of DIC measured displacement u_y,

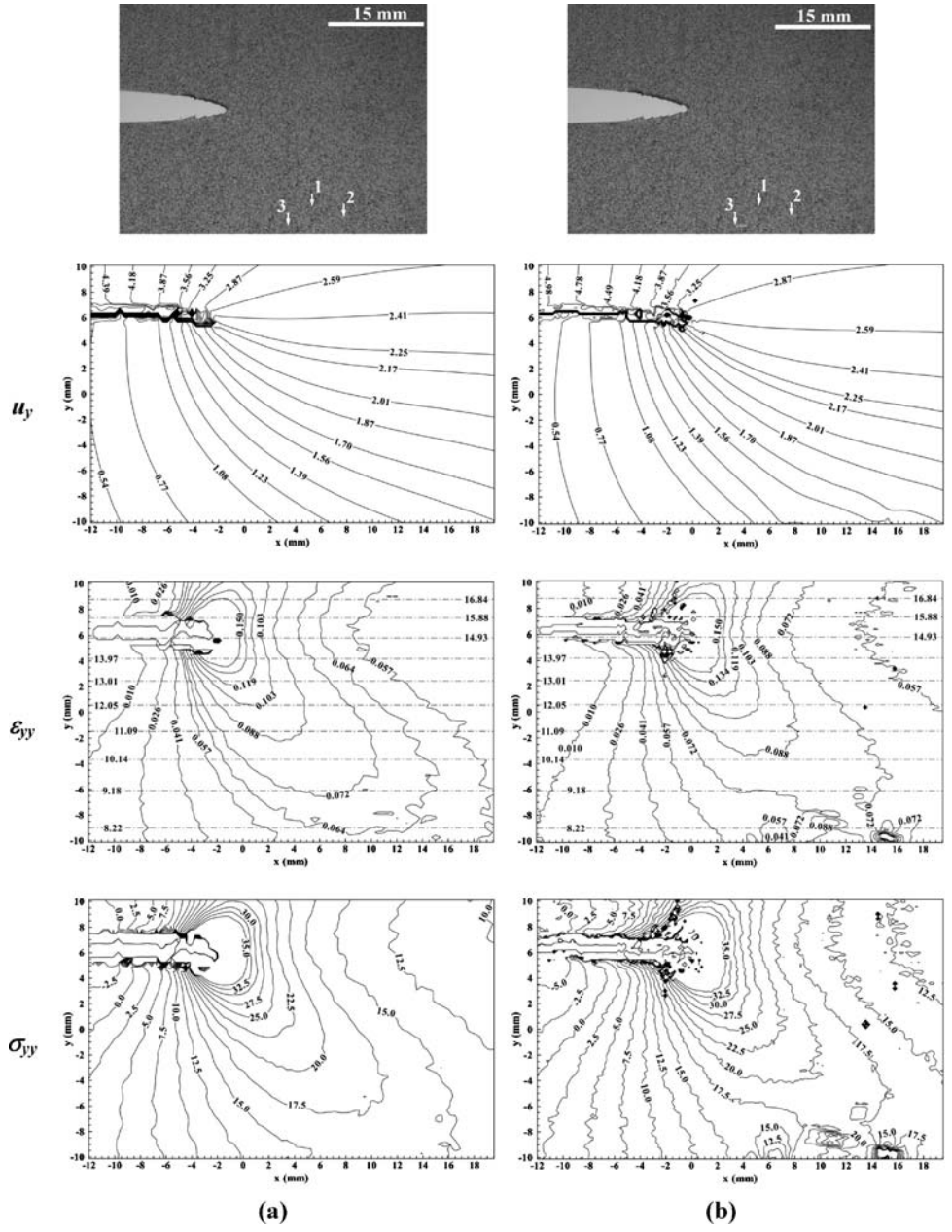

Fig. 13. New crack formation in FGM IV: (**a**) before crack nucleation (**b**) crack nucleation (**c**) crack growth and (**d**) crack coalescence

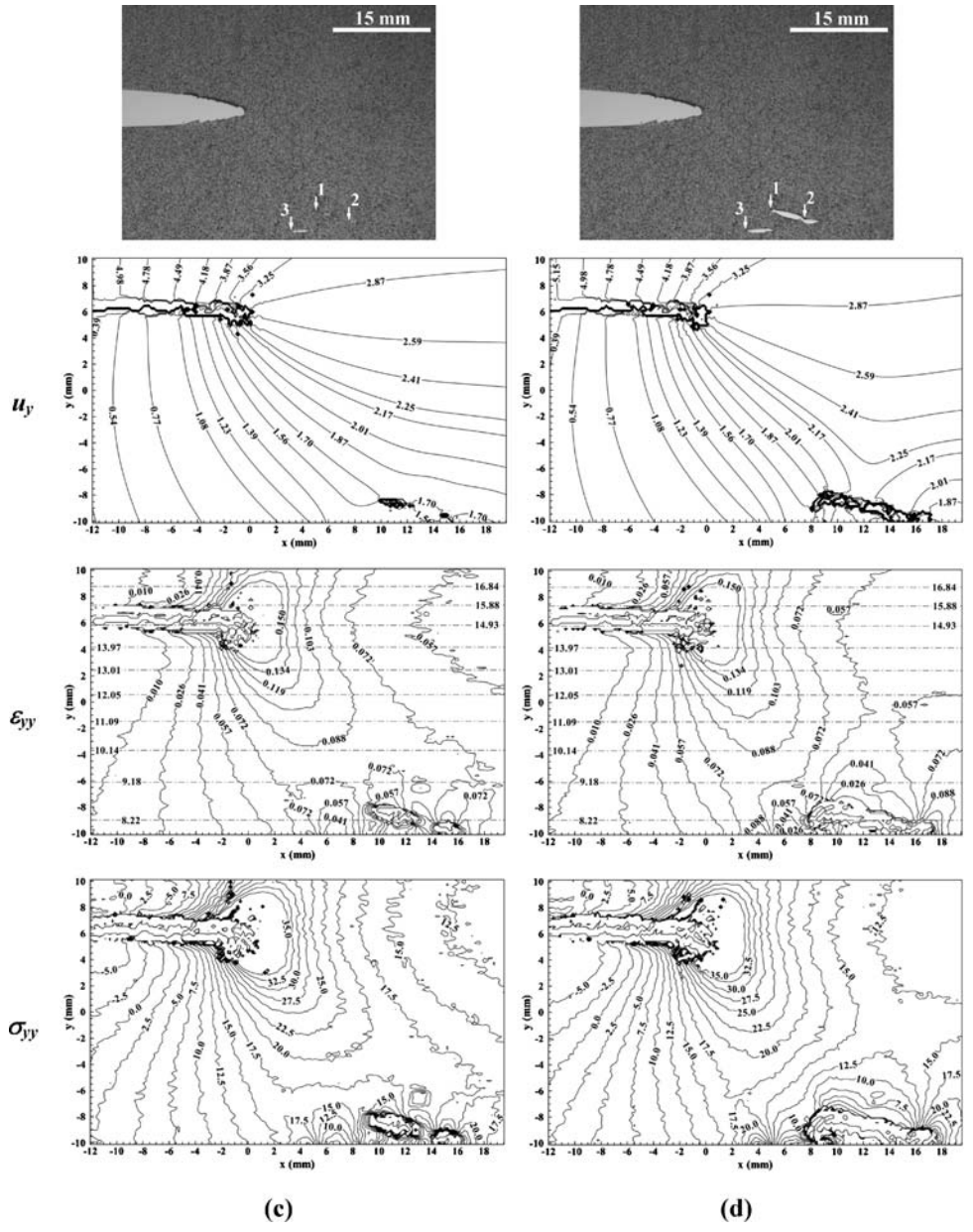

Fig. 13. Continued

normal strain ε_{yy}, and opening stress σ_{yy} (computed from DIC taking into account the spatial variation of elastic modulus) are shown in Fig. 13. The spatial variation of the failure stress has also been included as dash-dotted lines in the plot of the ε_{yy} field, with ε_{yy} in mm/mm and ε_f in percentage. The failure stress is 8.22 MPa everywhere in the region shown in Fig. 13. Figure 13(a) corresponds to an instant before the formation of any new crack and no stress concentration, other than that caused by the initial crack, is visible. In addition, the strain levels are generally below the local failure strain. As load increases, Fig. 13(b) shows the nucleation of cracks 1 and 2 (crack 3 is just below our range of correlated displacements) and both stress and strain concentrations appear in the lower right corner of the field of view. Also, the strain level at the location of the two nucleated cracks has clearly reached the local failure strain of the material. In Fig. 13(c) we can see crack growth, while crack coalescence (between 1 and 2) is observed in Fig. 13(d). During the

entire process the initial crack, which continues blunting as seen from the four images in Fig. 13, grows by 2–3 mm but does not kink. These results show that when developing crack kinking theories for FGMs care needs to be taken to include local strength effects. The material gradient needs to be comparable to the fracture process zone in order to have an effect on kinking, but if the gradient between brittle and ductile regions is very large spontaneous crack nucleation away from dominant stress singularities can occur. This very interesting effect which would not occur in materials with homogeneous elastic *and* failure properties, demonstrated here experimentally, was also seen numerically in the work of Kandula et al. (2004) and is currently the focus of further study.

Conclusions

The aim of this experimental investigation was to study the fracture response of FGMs under mixed mode loading and investigate the suitability of existing criteria for homogeneous materials (such as maximum hoop stress or energy release rate) to predict crack kinking in graded materials. Polymeric ECO-based quasi-brittle homogeneous and graded materials were manufactured and mechanically characterized in detail using uniaxial tensile tests, and fracture tests based on the full-field digital image correlation (DIC) technique. The detailed characterization of the materials coupled with full-field optical diagnostics allowed a comprehensive analysis of the role of all relevant parameters. Mixed mode loading conditions in the FGMs were generated by applying inclined external in-plane load, by inclining the crack at an angle to the property gradient, and by a combination of both. Several conclusions can be drawn from this work:

1. The effect of property gradient induced mixity is small if the inherent material length scale is much larger than the process zone size.
2. In such cases, crack kinking is well predicted by the homogenous criteria of (generalized) maximum hoop stress or energy release rate, provided the effect of T-stress is taken into account in the computation of stress intensity factors when this become large.
3. For finite crack extensions in homogeneous materials the crack grows along the path that maximizes K_I and $K_{II} = 0$, while for the case of FGMs, the crack will grow towards a region of the FGM that exhibits lower fracture toughness, and along this path K_{II} is not necessarily equal to zero.
4. For FGMs possessing a steep property gradient subjected to mixed mode loading crack nucleation, growth, and coalescence can occur away from the main crack if the local failure properties dictate this. In such cases a criterion that compares the stress field surrounding the crack to local failure properties would be needed. This has significant implications in metal/ceramic FGM systems in which the toughness between metal and ceramic differ by several orders of magnitude while elastic properties differ much less.

Acknowledgments This work was supported by the National Science Foundation (grants CMS 01-15954 and CMS 02-96105). Hi-Cone, a Division of Illinois Tools Work Inc., generously provided the material.

References

1. Erdogan F, Sih GC (1963) On the crack extension in plates under plane loading and transverse shear. J Basic Eng-Trans ASME 85D(4):519–525.
2. Cotterell B (1965) On the brittle fracture paths. Int J Fract Mech 1(2):96–103.
3. Gu P, Asaro RJ (1997) Crack deflection in functionally graded materials. Int J Solids Struct 34(24):3085–3098.
4. Gu P, Asaro RJ (1997) Cracks in functionally graded materials. Int J Solids Struct 34(1):1–17.
5. Becker TL Jr, Cannon RM, Ritchie RO (2001) Finite crack kinking and T-stresses in functionally graded materials. Int J Solids Struct 38(32–33):5545–5563.
6. Kim J-H, Paulino GH (2003) T-Stress, mixed-mode stress intensity factors, and crack initiation angles in functionally graded materials: a unified approach using the interaction integral method. Comput Methods Appl Mech Eng 192(11–12):1463–1494.
7. Chao YJ, Liu S, Broviak BJ (2001) Brittle fracture: variation of fracture toughness with constraint and crack curving under mode I conditions. Exp Mech 41(3):232–241.
8. Smith DJ, Ayatollahi MR, Pavier MJ (2001) The role of T-stress in brittle fracture for linear elastic materials under mixed-mode loading. Fatigue Fract Eng Mater Struct 24(2):137–150.
9. Rousseau C-E, Tippur HV (2000) Compositionally graded materials with cracks normal to the elastic gradient. Acta Mater 48(16):4021–4033.
10. He M-Y, Hutchinson JW (1989) Kinking of a crack out of an interface. J Appl Mech-Trans ASME 56:270–278.
11. Abanto-Bueno J, Lambros J (2005) Parameters controlling R-curves in functionally graded materials under mode I loading. Int J Solids Struct (In press).
12. Williams JG, Ewing PD (1972) Fracture under complex stresses—the angled crack problem. Int J Fract 8(4):416–441.
13. Andrady AL (1990) Weathering of polyethylene (LPDE) and enhanced photodegradable polyethylene in the marine environment. J Appl Polym Sci 39(2):363–370.
14. Lambros J, Santare MH, Li H, Sapna GH III (1999) A novel technique for the fabrication of laboratory scale model functionally graded materials. Exp Mech 39(3): 184–190.
15. Ivanova E, Chudnovsky A, Wu S, Sehanobish K, Bosnyak

CP, Wu S (1996) A new experimental technique for modeling of a micro-heterogeneous media. Exp Tech 20(6):11–13.
16. Li H, Lambros J, Cheeseman BA, Santare MH (2000) Experimental investigation of the quasi-static fracture of functionally graded materials. Int J Solids Struct 37(27): 3715–3732.
17. Abanto-Bueno J, Lambros J (2002) Investigation of crack growth in functionally graded materials using digital image correlation. Eng Fract Mech 69(14–16):1695–1711.
18. Sutton MA, Wolters WJ, Peters WH, Ranson WF, McNeill SR (1983) Determination of displacements using an improved digital image correlation method. Image Vis Comput 1(3):133–139.
19. Bruck HA, McNeill SR, Sutton MA, Peters WH III (1989) Digital image correlation using Newton–Raphson method of partial-differential correction. Exp Mech 29(3): 261–267.
20. McNeil SR, Peters WH, Sutton MA (1987) Estimation of stress intensity factor by digital image correlation. Eng Fract Mech 28(6):101–112.
21. Eischen JW (1987) Fracture of nonhomogeneous materials. Int J Fract 34(1):3–22.
22. Delale F, Erdogan F (1983) The crack problem for a nonhomogeneous plane. J Appl Mech Trans ASME 50(3):609–614.
23. Abanto-Bueno J, Lambros J (2005) Experimental determination of cohesive failure properties of a photo-degradable copolymer. Exp Mech 45(2):144 –152.
24. Kandula SSV, Abanto-Bueno J, Geubelle PH, Lambros J (2005) Cohesive modeling of dynamic fracture in functionally graded materials. Int J Fract 132:275–296.